Chemical Physics 524 (2019) 63–69

Contents lists available at ScienceDirect

Chemical Physics

journal homepage: www.elsevier.com/locate/chemphys

Evidences for phase transition and metallization in β-In_2S_3 at high pressure

Kaixiang Liu[a,b], Lidong Dai[a,*], Heping Li[a], Haiying Hu[a], Linfei Yang[a,b], Chang Pu[a,b], Meiling Hong[a,b]

[a] Key Laboratory of High-Temperature and High-Pressure Study of the Earth's Interior, Institute of Geochemistry, Chinese Academy of Sciences, Guiyang, Guizhou 550081, China

[b] University of Chinese Academy of Sciences, Beijing 100039, People's Republic of China

ARTICLE INFO

Keywords:
High pressure
Phase transition
Metallization
Diamond anvil cell
Electrical conductivity

ABSTRACT

The high-pressure characteristics including structural phase transition, vibration and electronic transport of β-In_2S_3 up to 43.0 GPa are determined using a diamond anvil cell (DAC) combined with AC impedance spectroscopy, Raman spectroscopy, atomic force microscopy (AFM) and high-resolution transmission electron microscopy (HRTEM). A structural phase transition and a semiconductor-to-metal transition are observed at ~7 GPa and ~41.2 GPa, respectively. When the pressure is released from 43.0 GPa, a single amorphous state is observed from Raman spectroscopy. We determine that the phase transition of metallization is irreversible after decompression from the pressure above 40 GPa. However, when the sample is decompressed from the pressure below 10 GPa, the phase transition is reversible. The unique properties displayed by β-In_2S_3 under different experimental pressure ranges can be reasonably explained by its crystalline structure observable from the microscopic observations of HRTEM and AFM images.

1. Introduction

Indium sulfide (In_2S_3) belongs to the A_2B_3-type chalcogenides. Indium sulfide contains polymorphic phases composed of the defect spinel cubic α phase (*Fd3m*, Z = 8, S.G:227), defect spinel tetragonal β-phase ($I4_1/amd$, Z = 1, S.G.:141) and layered structure trigonal γ-phase (*P3m*1, Z = 1, S.G: 164) [1–3]. As the most stable phase of indium sulfide at ambient conditions, the β-phase of In_2S_3 will transform into the α-phase with a cubic crystalline structure at temperatures higher than 693 K and then will further transform into the γ-phase with a trigonal crystalline structure above 1027 K [3]. Each individual unit cell of β-In_2S_3 with the deficient spinel structure ($I4_1/amd$, $Z = 16$) is made up of 80 atoms of indium and sulfur. The anionic sulfur forms the distortedly cubic closed-spaced sublattice, in which the cationic indium occupies the octahedral and 2/3 of the tetrahedral sites, and the rest 1/3 of the tetrahedral sites are vacancies [3,4].

Because of the good photoconductive and photoluminescent properties, β-In_2S_3 with a direct band gap of 1.9–2.9 eV [5–7] has attracted great interest owing to its fundamental material properties, such as crystal structure, optical properties and electronic band structure [8–10]. High pressure is an efficient method to change and tune the distance and interaction among atoms or molecules, and can result in the occurrence of a structural phase transition and metallization process. Previously reported studies on β-In_2S_3 at high-pressure have mainly focused on the crystalline structural parameters and phase stability on the basis of *in-situ* high-pressure synchrotron X-ray diffraction (XRD) and electrical transport measurements in a diamond anvil cell [11–14]. Yao et al. [11] reported that a phase transition from a tetragonal to cubic crystalline structure started at 7.1 GPa and was completed at 23.6 GPa for nanocrystalline β-In_2S_3 with the grain size of 5–6 nm using silicone oil as the pressure transmitting medium. Lai et al. [12] observed two pressure-induced phase transitions of β-In_2S_3 at ~6.6 GPa and 11.1 GPa accompanied by a new polymorph with the structure of a cubic defect Th_3P_4 after laser heating at the pressure of 35.6 GPa, using the pressure transmitting medium of LiF, silicone oil and NaCl. According to previous studies reported by Li et al. [13,14], a stable phase of β-In_2S_3 was observed up to 41.3 GPa using *in-situ* high-pressure synchrotron XRD [13]; however, a drastic variation of resistivity and a pressure-induced metallization of the sample were detected at ~6.8 GPa using *in-situ* high-pressure electrical transport measurements [14].

It has been proposed that the high-pressure vibrational characteristic parameter variations of the Raman peak and Raman mode can be used to extrapolate the structural phase transition, amorphization and metallization for the A_2B_3 compound [15,16]. The measurement of electrical conductivity is one of the most effective methods to

* Corresponding author.
E-mail address: dailidong@vip.gyig.ac.cn (L. Dai).

https://doi.org/10.1016/j.chemphys.2019.04.025
Received 27 February 2019; Received in revised form 24 April 2019; Accepted 24 April 2019
Available online 25 April 2019
0301-0104/

distinguish between semiconductors and metals [15–17]. Thus, further systematic investigation of the electrical properties and Raman spectroscopy at high pressure is required to determine whether a pressure-induced phase transition occurs for β-In_2S_3.

In the present study, to investigate the pressure-induced phase transition and metallization of β-In_2S_3, we determined the electrical and structural properties at pressures up to 43.0 GPa using a diamond anvil cell (DAC) in conjunction with AC impedance spectroscopy, Raman spectroscopy, atomic force microscopy (AFM) and high-resolution transmission electron microscopy (HRTEM). Furthermore, the corresponding phase transition, metallization and amorphization of β-In_2S_3 at high pressure are discussed in detail.

2. Experimental details

High-purity β-In_2S_3 powder (99.999%) was acquired from the Alfa-Aesar company. A DAC with an anvil culet of 300 μm was adopted to perform the high-pressure Raman spectroscopy experiments. A ruby single crystal with a grain size of ~5 μm was used for pressure calibration. Helium was used as the pressure medium to provide a hydrostatic environment, and no pressure medium was used for the non-hydrostatic environment. The excitation laser power was typically 20 mW for collection of the Raman spectra and 0.5–40 μW for that of the fluorescence. Spectra were recorded in the backscattering geometry using an argon ion laser (Spectra physics; 514.5 nm, power < 1 mW) in the range 100–500 cm^{-1} with a spectral resolution of 1.0 cm^{-1}. To avoid pressure oscillation, the DAC pressure equilibration time was 1 h at each pressure point before spectral acquisition. To determine the positions of the Raman modes and its uncertainty, the corresponding Raman spectra were fitted by a Lorenz-type function using the PeakFit software. The AFM and TEM data were obtained with a Multimode 8 mass spectrometer (Bruker) and a Tecnai G2 electron microscope (F20 S-TWIN TMP) respectively.

For the high-pressure electrical conductivity experiments, the sample was crushed into a powder (~2 μm). A T-301 stainless steel gasket was pre-indented to a thickness of ~60 μm and a 180-μm hole was drilled with a laser. A 100-μm hole was drilled as an insulating sample chamber after a mixture of boron nitride powder and epoxy was compressed into the hole. Fig. 1 shows the cross-sectional assembly of the DAC used in this study. The Solartron-1260 and Solartron-1296 impedance spectroscopy analyzers were used to perform AC impedance spectroscopy measurements in the frequency range 10^{-1}–10^{7} Hz. Detailed descriptions of the high-pressure equipment and experimental procedures can be found elsewhere [15–17].

3. Results and discussion

The Raman scattering experiment is widely applied to efficiently explore the high-pressure phase stability and vibrational information [15,16]. In Fig. 2, the Raman spectra of β-In_2S_3 obtained at room temperature up to ~43.0 GPa under non-hydrostatic environment are shown. Nine typical Raman vibration modes of β-In_2S_3 were observed at ambient pressures, which are consistent with previously reported experimental results [18–21]. According to the research of Lutz et al. [21], all of these representative peaks at 113, 135, 162, 178, and 326 cm^{-1} for β-In_2S_3 can be ascribed to the F_{2g} mode, and the peaks at 265 and 366 cm^{-1} were assigned to the E_g and A_{1g} modes, respectively. All of the A_{1g}, E_g and F_{2g} modes can be attributed as characteristic vibrations of the spinel structure [21]. The Raman spectrum of β-In_2S_3 is characterized by the presence of two strong peaks at approximately 246 and 306 cm^{-1}, where the peak at 246 cm^{-1} corresponds to the symmetric stretching vibration of InS_6 octahedral and the peak at 306 cm^{-1} corresponds to the symmetric stretching vibration of InS_4 tetrahedral [19]. Under the non-hydrostatic environment, all of the obtained Raman modes were continuously slightly shifted towards higher frequencies with increasing pressure. When the pressure was increased up to 6.8 GPa, some remarkable variations were detected in the Raman spectrum of β-In_2S_3. All of the typical Raman vibration modes of β-In_2S_3 disappeared except for the characteristic Raman mode of β-In_2S_3 with the peak at 306 cm^{-1}, and at the same time, three new Raman modes appeared at the pressure of 6.8 GPa (the peaks at 126, 237 and 373 cm^{-1}). All of these new Raman modes shifted to higher frequencies with increasing pressure, and then disappeared at higher pressure (above 9.8 GPa for the Raman modes with peak positions of 237 and 373 cm^{-1}, above 23.8 GPa for the Raman mode with a peak position of 126 cm^{-1}). All of the varied characteristics in the Raman spectrum of β-In_2S_3 at ~7 GPa may be concerned with the structural phase transition that has been reported previously. As for the Raman modes that disappeared at higher pressure, these may be related to the pronounced broadening trend of the Raman modes with increasing pressure, which has also been observed for other A_2B_3-type structural chalcogenides under high pressure [15,22]. When the pressure was enhanced up to 43.0 GPa, the Raman modes exhibited pronounced broadening, to result in only one characteristic Raman mode. These remarkable variations in the Raman spectra of β-In_2S_3 above ~7 GPa indicated that this compound may undergo a pressure-induced phase transition. Upon further decompression from 43.0 GPa, a single amorphous state was observed, which is consistent with the high-pressure synchrotron X-ray diffraction results reported by Lai et al. [12]. However, the recovered sample showed an excellent crystalline phase upon decompression from a relatively lower pressure (~7.8 GPa).

The variations of the experimental Raman-active mode frequencies of β-In_2S_3 with increasing pressure under non-hydrostatic environment are shown in Fig. 2(b). All of these obtained Raman modes at ambient pressure exhibited a simple monotonic linear relationship with the pressure under our experimental conditions. The obtained fitting results and the pressure coefficients are summarized in Table 1 using the equation$\omega(P) = \omega_0 + \alpha P$. In the progress of compression, all of the observed Raman modes could be divided into two intervals: below ~7.0 GPa and above ~7.0 GPa. We acquired nine relatively small $\partial\omega/$

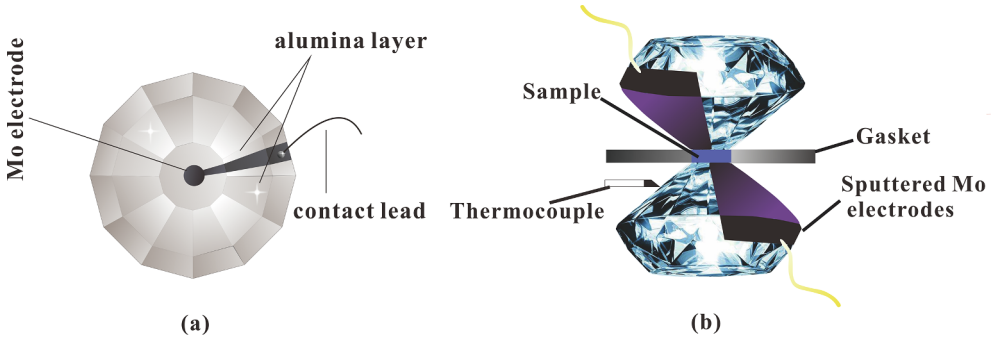

Fig. 1. Experimental assemblage for high-pressure electrical conductivity measurement for β-In_2S_3. (a) Configuration of plate electrodes integrated between two symmetric diamond anvils. (b) Cross section of the DAC used for impedance spectroscopy measurement at high pressure.

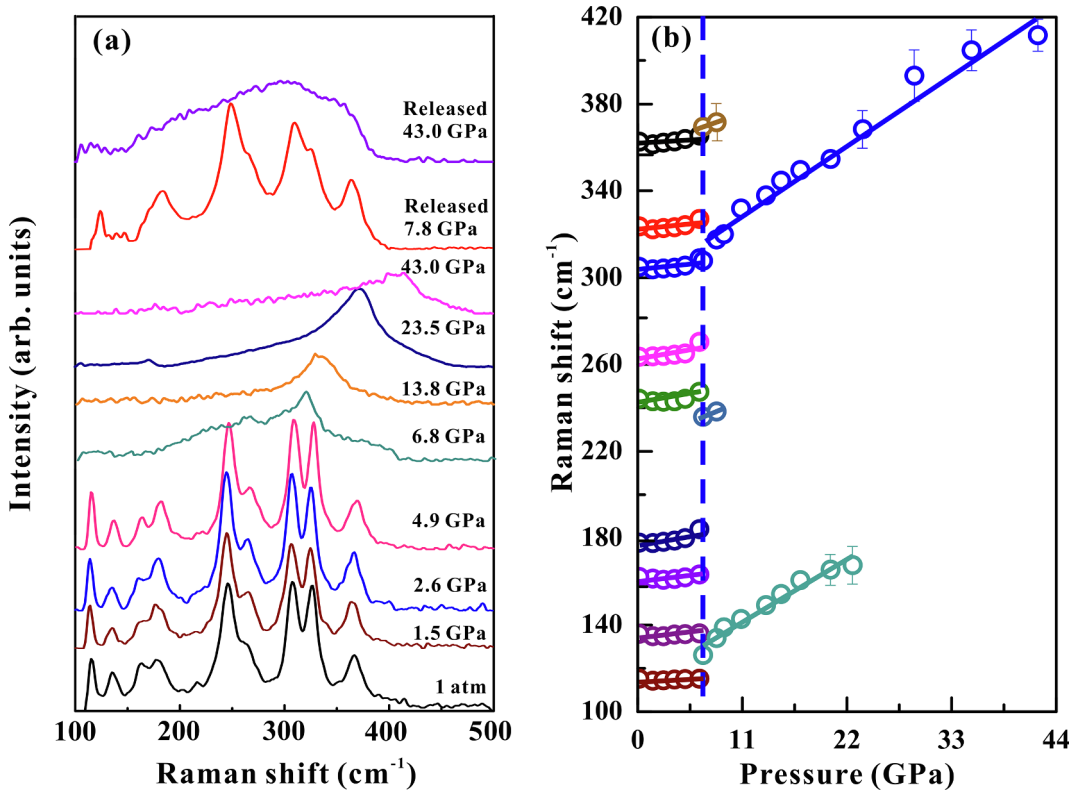

Fig. 2. Raman spectroscopic results of β-In_2S_3 at high pressure under non-hydrostatic environment. (a) Raman spectra at each selected pressure (λ = 514 nm and T = 300 K). (b) Linear relationship between Raman shift of β-$In_2S_3$and pressure. Errors in both frequency and pressure are within the size of symbol.

Table 1
Pressure dependence of the Raman shift for β-In_2S_3 under nonhyd-rostatic and hydrostatic environments. The peaks at the peaks at 126, 237 and 373 cm^{-1} are the new Raman modes appeared at ~7.0 GPa.

Pressure condition	$\omega(P)(cm^{-1})$	$\partial\omega/\partial P(cm^{-1}GPa^{-1})$ < 7.0 Ga	$\partial\omega/\partial P(cm^{-1}GPa^{-1})$ > 7.0 GPa
Nonhydrostatic	113	0.07	–
	126	–	2.43
	135	0.10	–
	162	0.19	–
	178	0.92	–
	237	–	1.80
	246	0.64	–
	265	1.47	–
	306	0.60	3.11
	326	1.14	–
	366	0.98	–
	373	–	1.42
Hydrostatic	113	0.08	–
	126	–	2.48
	135	0.10	–
	162	0.01	–
	178	0.24	–
	237	–	2.05
	246	0.33	–
	265	0.32	–
	306	0.29	3.06
	326	0.55	–
	366	0.56	–
	373	–	1.85

∂P (between 0.07 and 0.47 cm^{-1} GPa^{-1}) values below ~7.0 GPa, while four relatively large $\partial\omega/\partial P$ values (between 1.80 and 3.11 cm^{-1} GPa^{-1}) were disclosed above ~7.0 GPa. The shortening of the bond distance is known to cause a Raman frequency increase, while the enlargement of the equilibrium angle is known to lead to a decrease in Raman frequency. All of the positive $\partial\omega/\partial P$ values indicated a pressure-induced contraction for the distance of atoms in β-In_2S_3 in the progress of compression.

Previous studies concerning the pressure-induced phase transition of β-In_2S_3 at room temperature are inconsistent [11–14]. For example, Yao et al. [11] reported that a pressure-induced tetragonal to cubic phase transitions started at 7.1 GPa and was completed at 23.6 GPa for β-In_2S_3. Lai et al. [12] observed two pressure-induced phase transitions at ~6.6 GPa and 11.1 GPa. However, according to the previous study reported by Li et al. [13], a stable phase of β-In_2S_3 was detected up to 41.3 GPa. For a comprehensive consideration of the previously reported results by Yao et al. [11] and Lai et al. [12], the phase transition of β-In_2S_3 was detected by the variations in the synchrotron X-ray diffraction pattern. However, the observed changes from the synchrotron X-ray diffraction experiments reported by Li et al. [13] were too weak to cause the occurrence of a phase transition. To explore the potential deviatoric stress effect, we also measured the Raman spectra of β-In_2S_3 under hydrostatic environment. As shown in Fig. 3, both the Raman spectra and the Raman mode frequency evolution against pressure reveal the presence of a high-pressure phase for β-In_2S_3 above ~7.0 GPa. Additionally, the $\partial\omega/\partial$P values under hydrostatic environment disclosed in Table I also provided evidence for the structural phase transition. Similar as in non-hydrostaticity environment, the Raman spectrum returned to its original state when the pressure was released to ambient conditions from 8.6 GPa in hydrostatic environment.

To further verify the structural phase transition and determine the potential metallization of β-In_2S_3 under high pressure, the pressure-induced electrical conductivity measurements were conducted up to ~42.0 GPa at room temperature. Fig. 4(a)–(c) show the representative Nyquist plots of the impedance spectra of β-In_2S_3 under high pressure. The ZView software was adopted for equivalent circuit fitting of the plots. All the measured impedance spectra displayed a semicircle centered on the real axis (Z') in the high frequency range and an oblique small low-frequency tail. The semicircular arc in the high-frequency

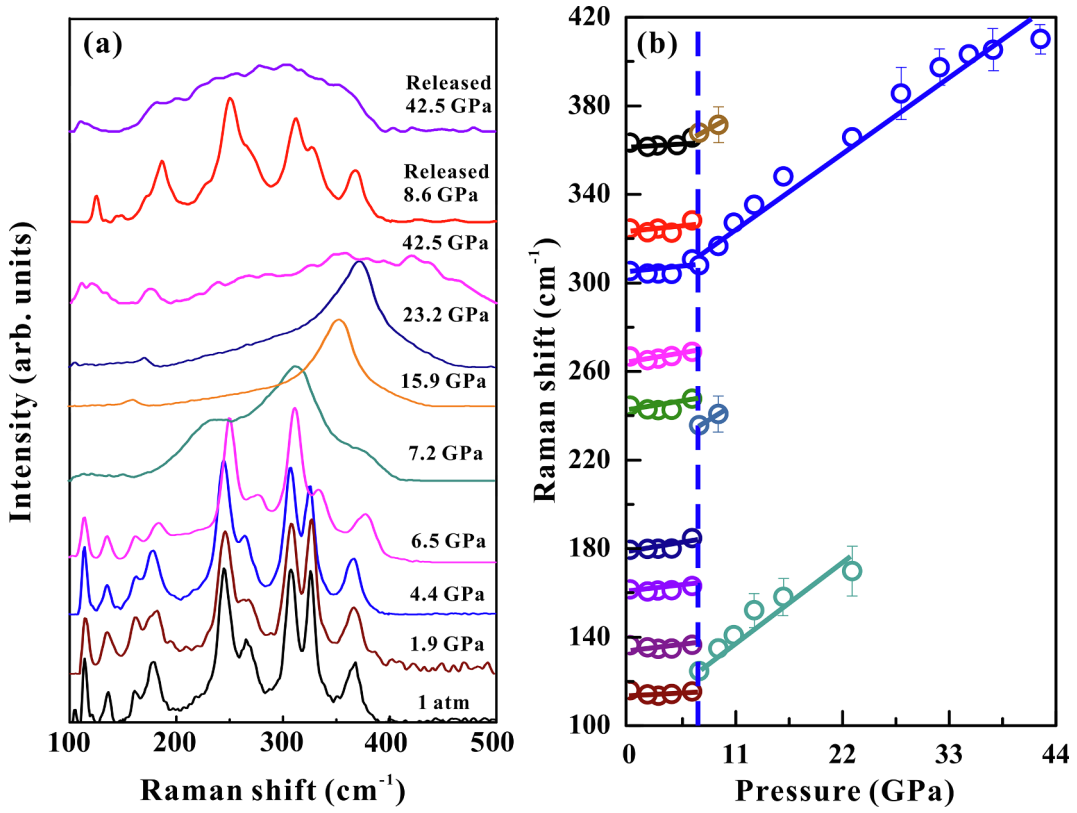

Fig. 3. Raman spectroscopic results of β-In_2S_3 at high pressure under hydrostatic environment. (a) Raman spectra at each selected pressure (λ = 514 nm and T = 300 K). (b) Linear relationship between Raman shift of β-$In_2S_3$and pressure. Errors in both frequency and pressure are within the size of symbol.

represented the bulk conduction of the sample, whereas the oblique tail in the low frequency range was characteristic of the grain boundary and was not reflected in the intrinsic electrical properties of the sample [23,24]. Both the grain boundary and grain interior resistance gradually increased with the increasing pressure below 7.5 GPa. After that, they showed a remarkable decreasing trend. When the pressure was increased to 26.2 GPa, only one impedance arc of the grain interior was observed in the fourth quadrant. This meant that some redundant connected electric charges arose in the sample, which was perhaps related to the pressure-induced spontaneous electrical polarization of the sample [25]. In this work, particular attention was focused on the varied contribution of the grain interior related to the pressure-induced structural phase transitions and metallization.

The electrical conductivity of the sample can be obtained as follows:

$$\sigma_b = \frac{1}{R_b}\left(\frac{l}{A}\right) \quad (1)$$

where A and l refer to the electrode area and the distance between the two electrodes, respectively. The pressure-dependent logarithm of the electrical conductivity of β-In_2S_3 in the process of compression and decompression at room temperature is shown in Fig. 4(d). A most obvious pressure–related effect was observed at ~7 GPa, where the electrical conductivity of β-In_2S_3 underwent a reversal in the pressure dependence. The electrical conductivity of β-In_2S_3 decreases gradually from ambient pressure to ~7 GPa, and showed a dramatically different increasing trend above ~7 GPa. When the pressure was increased above ~35 GPa, the electrical conductivity of β-In_2S_3 remained stable with a relatively large value, which may have been indicative of metallization. Furthermore, the high electrical conductivity was maintained for an extended period when the pressure was released to atmospheric pressure. Although some inconsistences exist on the structural phase transition of β-In_2S_3 at high pressure and room temperature from previous studies [11–14], the sudden change of the electrical conductivity for β-In_2S_3 at ~7.0 GPa could be attributed to a pressure-induced structural phase transition. In addition, a relatively low electrical conductivity value for β-In_2S_3 before and after the structural phase transition at ~7.0 GPa still maintained the a typical semiconductor characteristics, which is contrary to the previously acquired results from electrical transport reported by Li et al. [14].

A series of temperature-dependent conductivity measurements were carried out to determine whether β-In_2S_3 undergoes pressure-induced irreversible metallization. The obtained results for β-In_2S_3 were found to be well fitted by the Arrhenius equation. Below 41.2 GPa, a positive relationship between the electrical conductivity of β-In_2S_3 and the temperature was obtained, which disclosed a typical semiconductor behavior. β-In_2S_3 then showed a negative relationship with the temperature when the pressure was increased to 41.2 GPa. Free electrons are known to play an important role in the conduction process in metals. The improved scattering effect on free electrons induced by vibration of the crystal lattice, by increasing temperature will reduces the electrical conductivity. Therefore, all of these results clearly revealed that β-In_2S_3 suffers pressure-induced metallization at 41.2 GPa. In addition, it can be seen from Fig. 5(b) that β-In_2S_3 also exhibited typical metallic behavior after decompression to ambient pressure, which is also consistent with our previously reported results for Sb_2S_3 [15]. At a selected pressure, the activation energy of the sample can be obtained by

$$\sigma = \sigma_0 \exp(-E_t/k_b T) \quad (2)$$

where σ_0 denotes the pre-exponential factor (S m^{-1}), E_t denotes the activation energy (eV), k_b denotes the Boltzmann constant, and T denotes the absolute temperature (K). The E_t value can be determined by a linear fitting of the logarithmic conductivity as a function of 1000/T. The pressure dependence of the activation energy for β-In_2S_3 is shown in Fig. 5(c). The activation energy reflects the contributions to the mobile carriers from the effective defect energy level in the bandgap.

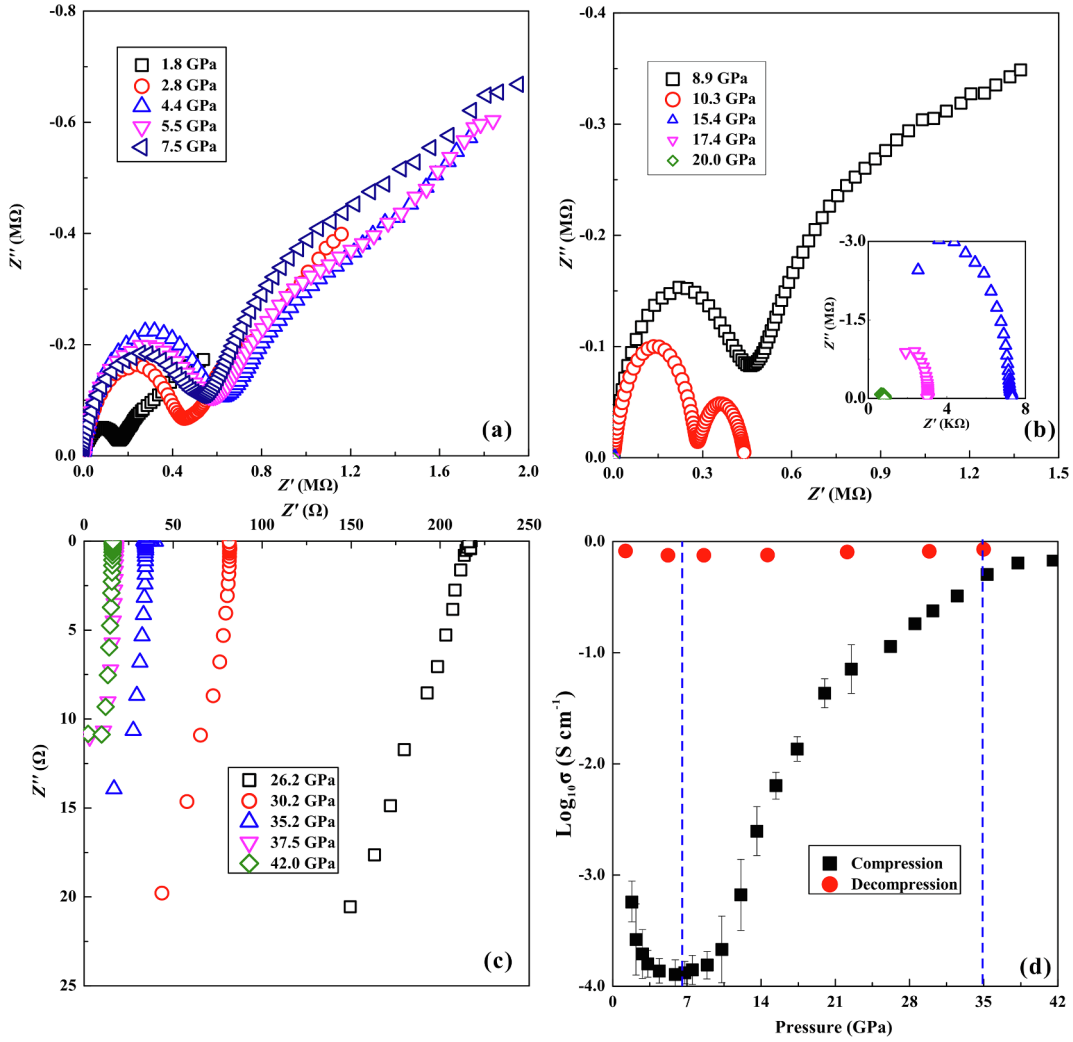

Fig. 4. (a)–(c) The representative Nyquist plots of impedance spectra for β-In_2S_3 at different pressures. (d) The relationship between the electrical conductivity of β-In_2S_3 and pressure in the process of compression and decompression.

The activation energy reduced with increasing pressure, which indicated that electrical transport of carriers became easier and the bandgap narrowed. The E_t value approached zero at the pressure of ~41.0 GPa, which meant a closing of the bandgap and appearance of the obvious metallization behavior i-n β-In_2S_3.

To further explore the influence of the pressure, some observations on the surface topography and microscopic structure of the recovered β-In_2S_3 were conducted through HRTEM and AFM. The typical images from the HRTEM and AFM results are shown in Fig. 6. From the image of HRTEM, we determined that the β-In_2S_3 layers had a distance of ~0.61 nm for the initial sample (Fig. 6(a)). The sample displayed a good preserved crystalline structure with a ~0.58 nm interlayer spacing upon decompression from 8.5 GPa (Fig. 6(b)). However, the structure was mostly disordered from the HTEM image of the sample decompressed from 44.3 GPa, and an amorphous state with an interlayer spacing of ~0.23 nm in the residual layered structure was also observed (Fig. 6(c)). Furthermore, the representative cross-sectional selected-area electron diffraction pattern of the recovered sample also revealed the crystalline and amorphous state of β-In_2S_3 upon decompression from 8.5 and 44.3 GPa, respectively. Fig. 6(d) and (e) displays the AFM images of the initial and recovered samples upon decompression from 8.5 GPa. There was no significant difference in the morphology of these two samples taking account of the size and space distribution of crystalline clusters, where both of them showed the available clusters of the crystalline shape clearly. As for the sample upon decompression from 44.3 GPa shown in Fig. 6(f), the surface morphology of β-In_2S_3 was completely destroyed, became lumpy and was significantly compacted. The diverse phenomenon caused by various pressures is consistent with our measured electrical conductivity and Raman spectroscopy results.

4. Conclusions

We have found that the phase transition and metallization of β-In_2S_3 occur at approximately 7.0 and 41.2 GPa, respectively. The results were obtained by a combination of experimental methods using DAC, including high-pressure Raman spectroscopy, temperature-dependent conductivity measurements, AFM and HRTEM. The structural phase transition at ~7.0 GPa manifests as noticeable changes in the Raman-active modes and the variation in slope of the conductivity. Furthermore, an irreversible semiconductor-to-metal transition occurs at ~42.5 GPa, which was determined by temperature-dependent conductivity measurements. The HRTEM and AFM images of the recovered sample upon decompression from 44.3 GPa confirm that β-In_2S_3 becomes an amorphous state with a permanent reduction in interlayer spacing of the residual layered structure. However, a reversible phenomenon of β-In_2S_3 is observed by virtue of the HRTEM, AFM images and Raman results when the pressure is released from below 10 GPa.

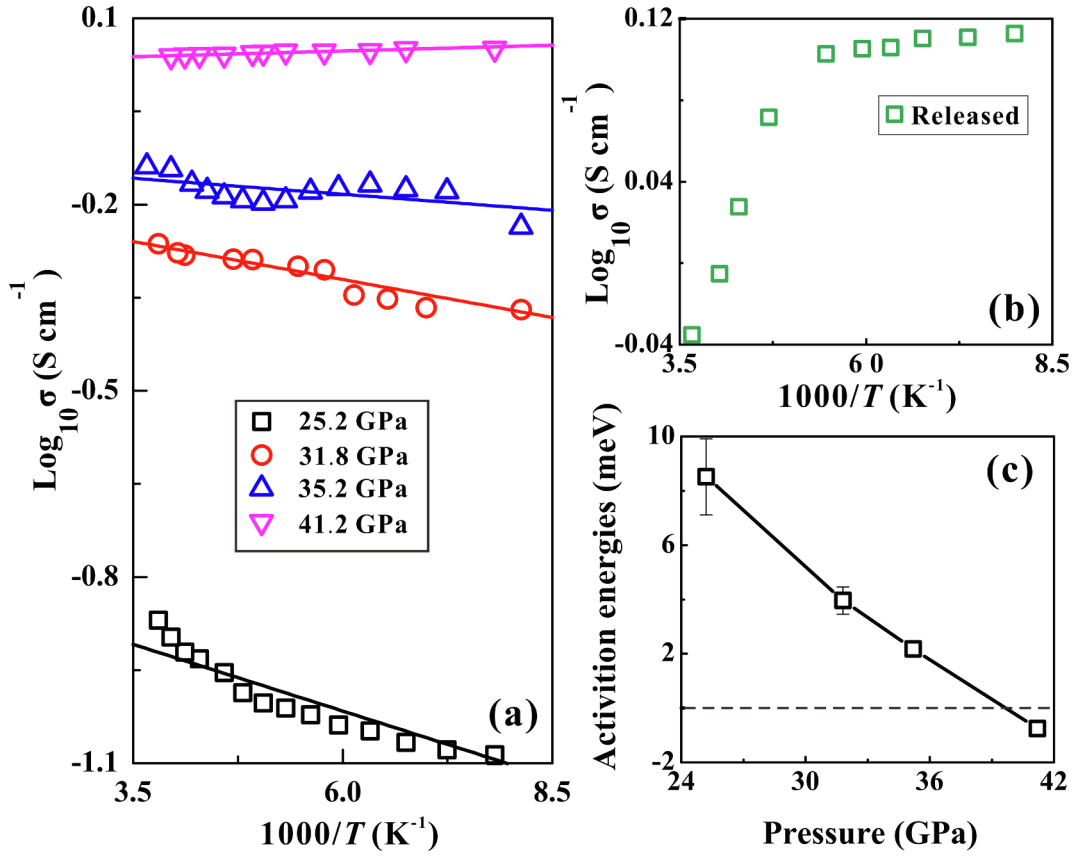

Fig. 5. (a) Electrical conductivity for β-In_2S_3 as a function of temperature at various pressure up to 41.2 GPa. (b) The metallic behavior of the decompressed β-In_2S_3. (c) The relationship between the activation energy of β-In_2S_3 and pressure.

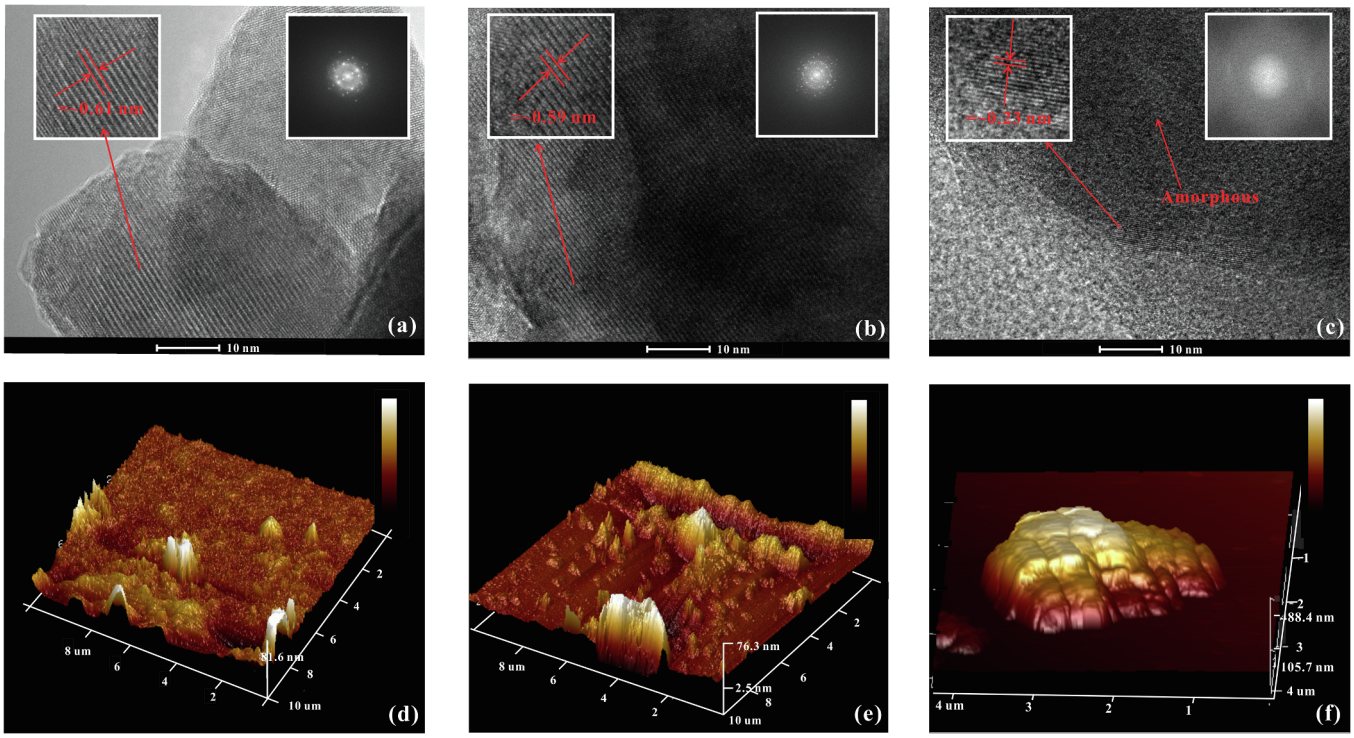

Fig. 6. (a) HRTEM images of β-In_2S_3 at ambient condition. (b) and (c) HRTEM images of the recovered sample decompression upon from 8.5 GPa and 44.3 GPa, respectively. Inset: the right one is cross-sectional selected-area electron diffraction patterns by HRTEM for the β-In_2S_3. Scale bars are 10 nm. (d) AFM image of β-In_2S_3 at ambient condition. (e) and (f) Pressure-induced morphology of decompressed β-In_2S_3 from 8.5 and 44.3 GPa, respectively.

Acknowledgements

This research was financially supported by the strategic priority Research Program (B) of the Chinese Academy of Sciences (18010401), Key Research Program of Frontier Sciences of CAS (QYZDB-SSW-DQC009), Hundred Talents Program of CAS, NSF of China (41774099 and 41772042), Youth Innovation Promotion Association of the Chinese Academy of Sciences (2019390), Special Fund of the West Light Foundation of the Chinese Academy of Sciences and Postdoctoral Science Foundation of China (2018M643532).

References

[1] R. Diehla, R. Nitsche, Vapour and flux growth of γ-In_2S_3, a new modification of insium sesquisulphide, J. Cryst. Growth. 20 (1973) 38–46.
[2] Y. Sharma, P. Srivastava, Electronic, optical and transport properties of $\alpha-$, $\beta-$ and $\gamma-$phases of spinel indium sulphide: an ab initio study, Mater. Chem. Phys. 135 (2012) 385–394.
[3] P. Pistor, J.M. Merino Álvarez, M. León, M. di Michiel, S. Schorr, R. Klenk, S. Lehmann, Structure reinvestigation of α−, β−and γ−In_2S_3, Acta. Crystallogr. B. 72 (2016) 410–415.
[4] E. Ghorbani, K. Albe, Role of oxygen and chlorine impurities in $\beta-In_2S_3$: A first-principles study, Phys. Rev. B. 98 (2018) 205201.
[5] W.T. Kim, C.D. Kim, Optical energy gaps of $\beta-In_2S_3$ thin films grown by spray pyrolysis, J. Appl. Phys. 60 (1986) 2631.
[6] Y.H. Kim, J.H. Lee, D.W. Shin, S.M. Park, J.S. Moon, J.G. Nam, J.B. Yoo, Synthesis of shape-controlled β-In_2S_3 nanotubes through oriented attachment of nanoparticles, Chem. Commun. 46 (2010) 2292.
[7] X. Xiong, Q. Zhang, L. Gan, X. Zhou, X.N. Xing, H.Q. Li, T.Y. Zhai, Geometry dependent photoconductivity of In_2S_3 kinks synthesized by kinetically controlled thermal deposition, Nano Res. 9 (2016) 3848.
[8] S.K. Batabyal, S.E. Lu, J.J. Vittal, Synthesis, Characterization and photocatalytic properties of In_2S_3, $ZnIn_2S_4$, and $CdIn_2S_4$ nanocrystals, Cryst. Growth. Des. 16 (2016) 2231–2238.
[9] S.H. Choe, T.H. Bang, N.O. Kim, H.G. Kim, Cl. Lee, M.S. Jin, W.T. Kim, Optical properties of β-In_2S_3 and β-In_2S_3: Co^{2+} single crystals, Semicond. Sci. Tech. 16 (2001) 98–102.
[10] A. Stoliaroff, N. Barreau, S. Jobic, C. Latouche, $\beta-In_2S_3$ for photovoltaic devices: investigation of the native point defects with ab initio first-principle calculations, Theor. Chem. Acc. 137 (2018) 102.
[11] B.B. Yao, H.Y. Zhu, S.M. Wang, P. Wang, M.Z. Zhang, The pressure-induced phase transition studies of In_2S_3 and In_2S_3: Ce nanoparticles, J. Solid. State. Chem. 210 (2014) 150–154.
[12] X.J. Lai, F. Zhu, Y. Wu, R. Huang, X. Wu, Q. Zhang, K. Yang, S. Qin, New high-pressure polymorph of In_2S_3 with defect Th_3P_4-type structure, J. Solid. State. 210 (2014) 155–159.
[13] Y.Q. Li, Q.L. Wang, Y. Gao, B. Liu, C.X. Gao, Y.Z. Ma, Investigation on morphological properties of In_2S_3 by high pressure X−ray diffraction, Mater. Res. Express. 4 (2017) 085902.
[14] Y.Q. Li, Y. Gao, N. Xiao, P.F. Ning, L.Y. Yu, J.X. Zhang, P.J. Niu, Y.Z. Ma, C.X. Gao, Reversible metallization and carrier transport behavior of In_2S_3 under high pressure, AIP. Adv. 8 (2018) 115202.
[15] L.D. Dai, K.X. Liu, H.P. Li, L. Wu, H.Y. Hu, Y.K. Zhuang, L.F. Yang, C. Pu, P.F. Liu, Pressure−induced irreversible metallization accompanying the phase transitions in Sb_2S_3, Phys. Rev. B 97 (2018) 024103.
[16] L.D. Dai, Y.K. Zhuang, H.P. Li, L. Wu, H.Y. Hu, K.X. Liu, L.F. Yang, C. Pu, Pressure−induced irreversible amorphization and metallization with a structural phase transition in arsenic telluride, J. Mater. Chem. C. 5 (2017) 12157–12162.
[17] Y.K. Zhuang, L.D. Dai, L. Wu, H.P. Li, K.X. Liu, L.F. Yang, C. Pu, Pressure−induced permanent metallization with reversible structural transition in molybdenum disulfide, Appl. Phys. Lett. 110 (2017) 122103.
[18] Y. Xiong, Y. Xie, G. Du, X. Tian, Y. Qian, A novel in situ oxidization–sulfidation growth route via self-purification process to $\beta-In_2S_3$ dendrites, J. Solid. State. Chem. 166 (2002) 336–340.
[19] H.Z. Tao, S. Mao, G.P. Dong, H.Y. Xiao, X.J. Zhao, Raman scattering studies of the Ge–In sulfide glasses, Solid. State. Commun. 137 (2006) 408–412.
[20] E. Karber, K. Otto, A. Katerski, A. Mere, M. Krunks, Raman spectroscopic study of In_2S_3 films prepared by spray pyrolysis, Mater. Sci. Semicond. Process. 25 (2013) 137–142.
[21] H.D. Lutz, W. Becker, B. Muller, M. Jung, Raman single crystal studies of spinel type MCr2S4(M= Mn, Fe Co, Zn, Cd), MIn2S4(M= Mn, Fe Co, Ni), MnCr2–2xIn2xS4 and Co1−xCdxCr2S4, J. Raman Spectrosc. 20 (1989) 99–103.
[22] K.X. Liu, L.D. Dai, H.P. Li, H.Y. Hu, L.F. Yang, C. Pu, P.F. Liu, Phase transition and metallization of orpiment by Raman spectroscopy, electrical conductivity and theoretical calculation under high pressure, Materials 12 (2019) 748.
[23] L.D. Dai, H.Y. Hu, H.P. Li, L. Wu, K.S. Hui, J.J. Jiang, W.Q. Sun, Influence of temperature, pressure, and oxygen fugacity on the electrical conductivity of dry eclogite, and geophysical implications, Geochem. Geophys. Geosyst. 17 (2016) 2394–2407.
[24] H.Y. Hu, L.D. Dai, H.P. Li, W.Q. Sun, B.S. Li, Effect of dehydrogenation on the electrical conductivity of Fe−bearing amphibole: Implications for high conductivity anomalies in subduction zones and continental crust, Earth. Planet. Sci. Lett. 498 (2018) 27–37.
[25] Y.A. Kandrina, A.N. Babushkin, S.N. Shkerin, Y.Y. Volkova, Application of the AC impedance spectroscopy at high pressures: Electrophysical properties of sulfur, Defect. Diffus. Forum. 295 (2002) 208–209.